Acta Astronautica, Volume 177, December 2020, pp. 30-38
DOI:10.1016/j.actaastro.2020.06.051

Trajectory Planning for Hypersonic Reentry Vehicle Satisfying Deterministic and Probabilistic Constraints

Runqi Chai[a,*], Antonios Tsourdos[a], Al Savvaris[a], Senchun Chai[b], Yuanqing Xia[b]

[a]*School of Aerospace, Transport and Manufacturing, Cranfield University, Bedfordshire, MK43 0AL, United Kingdom*
[b]*School of Automation, Beijing Institute of Technology, Beijing 100081, PR China*

Abstract

The present work explores the optimal flight of aero-assisted reentry vehicles during the atmospheric entry flight phase with the consideration of both deterministic and control chance constraints. To describe the mission profile, a chance-constrained optimal control model is established. Due to the existence of probabilistic constraints (chance constraints), standard numerical trajectory planning algorithms cannot be directly applied to address the considered problem. Hence, we firstly present an approximation-based strategy to replace the probabilistic constraint by a deterministic version. In this way, the transformed optimal control model becomes solvable for standard trajectory optimization methods. In order to obtain enhanced computational performance, an alternative convex-relaxed optimal control formulation is also given. This is achieved by convexifying the vehicle nonlinear dynamics/constraints and by introducing a convex probabilistic constraint handling strategy. Numerical simulations are provided to demonstrate the effectiveness of these two chance-constrained optimization approaches and the corresponding probabilistic constraint handling strategies.

Keywords: Reentry vehicles, atmospheric entry, probabilistic constraints, trajectory planning, numerical simulations.

*Corresponding author
Email addresses: r.chai@cranfield.ac.uk (Runqi Chai), a.tsourdos@cranfield.ac.uk (Antonios Tsourdos), a.savvaris@cranfield.ac.uk (Al Savvaris), chaisc97@bit.edu.cn (Senchun Chai), xia_yuanqing@bit.edu.cn (Yuanqing Xia)

1. Introduction

Atmospheric entry trajectory optimization problems for hypersonic vehicles (HVs) have received a large amount of attention worldwide during the last decade and will continuously act as a main focus of the aerospace industry [1–4]. Generally speaking, this type of problem aims at searching a sequence of control profiles such that the HV can be steered from a specific starting point to a targeted final point while optimizing some particular performance indices. During the planning phase, it is also desired that multiple process constraints and/or waypoint constraints are satisfied, thereby making the problem more complicated. To design a promising trajectory planner, researchers and engineers have devoted significant amount of efforts [5, 6]. A large amount of attention has been paid to the development of classical "discretization + optimization" mode-based trajectory optimization algorithms such as the well-known Gauss pseudospectral method (GPM) [7], the hp-adaptive pseudospectral method [8], and various other improved versions [9–11]. In addition, in [12–17], different bio-inspired optimization techniques were reported to approximate the optimal control trajectory and multiple evolutionary strategies were designed to further improve the performance and robustness of these algorithms.

The aforementioned investigations are of particular importance to the development of entry trajectory optimization methods and the results reported in those works have successfully demonstrated the effectiveness of the designed approaches. However, these works mainly considered the problem as a deterministic optimization model. Actually in practice, some system equations or constraint functions might be perturbed by uncertain parameters [18–20]. In this case, the problem becomes nondeterministic and typical trajectory optimization methods cannot be directly applied to explore the optimal solutions. Therefore, different from most existing works that only consider deterministic model, in this paper we research trajectory optimization methods which have the capability to deal with noise-perturbed constraints for system variables.

It should be noted that the noise-perturbed state or control constraints are usually modeled as chance constraints and they can severely affect the behaviour of the optimal flight trajectory. One way to address problems entailing this type of constraint is to use the robust optimization (RO) [21, 22]. An important feature of applying the robust optimization is that any constraint violation is not accepted. Hence, it generally makes solving the optimization problem more

challenging, as the feasible solution space is significantly restricted. Moreover, the optimality of the obtained solution might be degraded since the RO always considers the worst case of the problem caused by the uncertain parameter. As an effective alternative, chance-constrained optimization (CCO) has recently gained more attention in aerospace-related applications. This type of algorithm aims to transform the probabilistic constraints to an approximated deterministic version. Compared to RO-based methods, the CCO allows constraint violation which is less than a certain level, thereby removing restrictions on the feasible solution space to some extend. Contributions reported to apply the CCO are available to review in the literature [23–25]. More precisely, the authors in [24] outlined an dual-loop CCO algorithm and successfully applied this algorithm to tackle benchmark CCO problems. A kernel density estimation-based CCO method was proposed in [25] and the authors have shown that this approach can be applied to address a class of trajectory optimization missions in aerospace field. Furthermore, an approximation-based approach, named split Bernstein method, was developed by Zhao and Kumar [26]. In their work, the original version of the Bernstein method has been modified by using a piecewise smooth approximation function. Subsequently, this approach was applied to solve typical chance-constrained optimal control examples.

After approximating the probabilistic constraints, the original problem is usually transcribed to a deterministic yet nonconvex optimization model. A potential problem is that the computation time required for solving a nonconvex CCO model is usually high and unpredictable. Fortunately, as suggested by many published works, several potentially-effective strategies are able to tackle this problem. Among them, one promising strategy is the convex relaxation-based algorithms. The application of convex relaxation or convex optimization techniques in the exploration of optimal flight path has received an increasing attention during the last five years [27–29]. For instance, considering the impact angle and dynamic pressure constraints, Liu et al. [27] structured a convex relaxation-based approach to search the optimal intercept trajectory of an aerodynamically controlled missile. Similarly, Wang and Grant [28] implemented a sequential convex programming approach to plan the planetary entry trajectory while optimizing the terminal velocity. Besides, the authors of [29] proposed a multi-phase convex optimization algorithm so as to plan optimal flight trajectories for reentry vehicles while simultaneously satisfying the non-fly zone and

waypoint constraints. Nevertheless, one primary motivation for using convex relaxation is that the resulting convex optimization problem can have guaranteed polynomial-time complexity, while other nonconvex optimization formulations are in general NP-hard. Hence we also devote efforts on applying convex relaxation-based approach to address the chance-constrained HV atmospheric entry problem.

In the present work, our main objectives lie in the following twofold. Firstly, we are interested in developing a CCO-based approach that is able to produce the optimal control command for the HV atmospheric entry flight while aggressively satisfying multiple path constraints and probabilistic constraints. Secondly, to meet the growing demand for online computation, we aim to develop a computationally-friendly CCO-based approach as an alternative. This is achieved by devoting significant efforts on transcribing the original optimal control model into a convexified version and introducing a convex chance constraint approximation strategy. Subsequently, the operation and effectiveness of the two algorithms will be demonstrated by executing simulations on the considered HV atmospheric entry problem.

The rest of this work is structured as follows. In Sec 2, the mathematical formulation of the HV atmospheric entry problem with different types of constraints is constructed. In Sec 3, a nonconvex chance-constrained trajectory optimization method is presented after introducing an approximation-based chance constraint handling strategy. Afterwards, an alternative method which takes advantage of convex optimization is established in Sec 4. Sec 5 provides a number of numerical simulation results, whereas some concluding remarks are summarised in Sec 6.

2. Atmospheric Entry Optimal Control Problem

2.1. Hypersonic Vehicle Dynamics and Constraints

Definitions/notations of parameters and variables appearing in the rest of this section are pre-summarised in Table I.

To describe the atmospheric entry flight, equations of motion for the HV are firstly constructed, which can be written as:

$$\dot{x} = f(x) + B(x)u \tag{1}$$

Table 1: Notations for variables

x, u:	System state and control variables
r, θ, ϕ:	Radial distance, longitude and latitude of the HV
V, γ, ψ:	Velocity, flight path angle and azimuth angle of the HV
σ, σ_c:	Actual and demanded bank angles
S, m:	Reference area and mass of the HV
C_L, C_D :	Aerodynamic lift and drag coefficients
ρ, g:	Density of the atmosphere and gravity acceleration
ρ_0, h_s	Sea-level air atmosphere density and density scale height
R_e, t	Radius of the Earth and mission time
L, D	Lift and drag forces
t_0, t_f	Starting and ending time points

where $x = [r, \theta, \phi, V, \gamma, \psi, \sigma] \in \mathbb{R}^7$ and $u = \sigma_c$. The terms $f(x) \in \mathbb{R}^7$ and $B(x) \in \mathbb{R}^7$ are in the form of:

$$f(x) = \begin{bmatrix} V \sin\gamma \\ \frac{V \sin\psi \cos\gamma}{r \cos\phi} \\ \frac{V \cos\psi \cos\gamma}{r} \\ -\frac{D}{m} - g \sin\gamma \\ \frac{L \cos\sigma}{mV} + (\frac{V^2 - gr}{rV}) \cos\gamma \\ \frac{L \sin\sigma}{mV \cos\gamma} + \frac{V}{r} \sin\psi \cos\gamma \tan\phi \\ K_\sigma \end{bmatrix} \tag{2}$$

$$B(x) = \begin{bmatrix} 0_{1\times 6} & -K_\sigma \end{bmatrix}^T \tag{3}$$

Notably the introduction of demanded bank angle variable σ_c can effectively smooth the actual bank angle profile [28, 30]. During the entry maneuver, the engine of the HV is switched off. As a result, the motion is mainly affected by the gravity acceleration g, and the aerodynamic forces such as the lift L and drag D. The equations used to calculate these forces, together with the

isothermal atmospheric model [3, 31], are summarised below:

$$\begin{cases} \rho = \rho_0 e^{-\frac{r-R_e}{h_s}} \\ L = \frac{C_L}{C_D} D \\ D = \frac{1}{2}\rho V^2 C_D S \end{cases} \tag{4}$$

In order to maintain a safe flight, the entry trajectory should be restricted in a relatively-narrow corridor. This is achieved by imposing three hard path constraints $g(x) \in \mathbb{R}^3$ including the heating rate $\dot{Q}$, dynamic pressure P_d, and load factor N_L:

$$g(x) = \begin{bmatrix} \dot{Q}(x) \\ P_d(x) \\ n_L(x) \end{bmatrix} = \begin{bmatrix} k_Q \rho^{0.5} V^{3.15} \\ \frac{1}{2}\rho V^2 \\ \frac{\sqrt{L^2+D^2}}{mg} \end{bmatrix} \leq \begin{bmatrix} \bar{Q} \\ \bar{P}_d \\ \bar{N}_L \end{bmatrix} \tag{5}$$

in which $\bar{g} = [\bar{Q}, \bar{P}_d, \bar{N}_L]$ stands for the allowable limits. Besides, for the considered problem, state and control boundary constraints and box constraints are required to be satisfied, which can be expressed by Eq.(6) and Eq.(7):

$$\begin{cases} x(t_0) = x_0 \\ x(t_f) = x_f \end{cases} \tag{6}$$

$$\begin{cases} \underline{x} \leq x \leq \bar{x} \\ \underline{u} \leq u \leq \bar{u} \end{cases} \tag{7}$$

In Eq.(6), $x_0 \in \mathbb{R}^7$ is specified as $[r_0, \theta_0, \phi_0, V_0, \gamma_0, \psi_0, \sigma_0]$, while $x_f \in \mathbb{R}^3$ is defined as $[r_f, V_f, \gamma_f]$.

It is worth mentioning that in practice, the control signal may be affected by some noises ξ. For example, we may not have a fixed maximum attainable control actuation level, thus resulting in probabilistic control path constraint. To represent this type of constraint, we use the following formulation:

$$Pr\{C(u, \xi) \leq \bar{C}\} \geq \epsilon \tag{8}$$

In Eq.(7), $Pr\{\cdot\}$ is the probability operator reflecting the probability of violating/meeting a noise-perturbed inequality (e.g., $C(u, \xi) \leq \bar{C}$) is below/above a certain risk level ϵ. For the considered problem, the bank angle chance constraint is written as

$$Pr\{\sigma_c + \xi_\sigma \leq \bar{\sigma}_c\} \geq \epsilon_\sigma \tag{9}$$

where $\bar{\sigma}_c$ is the upper bound for σ_c. ξ_σ and ϵ_σ denote, respectively, the uncertain parameter acted on the demanded bank angle and the permissible risk level.

2.2. Atmospheric Entry Optimal Control Model

Apart from the modeling of system dynamics and constraints, the mission objective function J should be specified. If it is desired to complete the entire entry maneuver in the shortest time possible, the terminal time point t_f can be selected to minimize. That is,

$$J_1 = t_f \tag{10}$$

Alternatively, if we want to obtain an entry trajectory with the maximum cross-range, the objective function can be defined as:

$$J_2 = -\phi_f \tag{11}$$

where $\phi_f = \phi(t_f)$ represents the value of latitude at the terminal time point t_f. Consequently, according to Eqs.(1)-(11), the overall HV atmospheric entry trajectory optimization problem can be formulated as:

$$\begin{aligned} \text{minimize} \quad & J_1 \quad \text{or} \quad J_2 \\ \text{subject to} \quad & \dot{x} = f(x) + B(x)u \\ & x(t_0) = x_0 \\ & x(t_f) = x_f \\ & \underline{x} \leq x \leq \bar{x} \\ & g(x) \leq \bar{g} \\ & Pr\{C(u, \xi) \leq \bar{C}\} \geq \epsilon \end{aligned} \tag{12}$$

3. Nonconvex Chance-Constrained Optimization Approach

This section presents a nonconvex chance-constrained optimization (NCCO) approach that is capable of searching the optimal solution for the nondeterministic atmospheric entry trajectory optimization problem constructed in Sec 2.

3.1. Handling the Probabilistic Constraint

In recent years, various effective trajectory optimization algorithms have been proposed in the literature. However, it is important mentioning that most of these reported algorithms cannot be directly applied to search the solution of the optimization model (12). This is because existing algorithms or solvers mainly target at deterministic optimization model, while problem (12) is non-deterministic due to the existence of probabilistic constraint. Therefore, motivated by the work presented in [23], a proper treatment of the noise-perturbed

constraint (8) or (9) is performed. To clearly show how this chance-constraint handling strategy works, general steps are summarised as follows:

Step 1. Perform an initial transformation on Eq.(8) via $P(u) = Pr\{C(u,\xi) \leq \bar{C}\}$=$1 - Pr\{C(u,\xi) > \bar{C}\}$.

Step 2. Rewrite $P(u)$ in the form of (13) by considering $C(u,\xi) \leq \bar{C}$ as an event

$$P(u) = 1 - \mathbb{E}(H(C(u,\xi))) \tag{13}$$

where $\mathbb{E}$ stands for the expectation, whereas the H function is in the form of (14).

$$H(C(u,\xi)) = \begin{cases} 1 & \text{if} \quad C(u,\xi) \leq \bar{C} \\ 0 & \text{if} \quad C(u,\xi) > \bar{C} \end{cases} \tag{14}$$

Step 3. Reformulate the original probabilistic constraint by:

$$\mathbb{E}(H(C(u,\xi))) \leq 1 - \epsilon \tag{15}$$

Step 4. Define an approximation function $\Xi(k, C(u,\xi))$ in the form of

$$\Xi(k, C(u,\xi)) = \frac{m_1 + k}{m_2 e^{-kC(u,\xi)} + k} \tag{16}$$

Step 5. Replace $H(\cdot)$ in Eq.(15) by $\Xi(k, C(u,\xi))$ and approximate the control chance constraint as

$$\mathbb{E}(\Xi(k, C(u,\xi))) \leq 1 - \epsilon \tag{17}$$

Remark 1. In step 4 and step 5, the defined approximation function is applied to replace the unit jump function $H(\cdot)$ in Eq.(15). It can be verified that $\Xi(k, C(u,\xi))$ is an aggressive approximation of $H(C(u,\xi))$ and $\Xi(k, C(u,\xi))$ is strictly greater than $H(C(u,\xi))$. In addition, an advantage of using the approximation function (16) instead of $H(\cdot)$ is that this function is smooth and differentiable on the solution space, which means it tends to result in less numerical difficulties for the gradient-based optimization algorithms.

3.2. Deterministic NCCO Model

To calculate the expectation value of $\Xi(k, C(u,\xi))$ (e.g., $\mathbb{E}(\Xi(k, C(u,\xi)))$), the widely-applied Markov chain Monte-Carlo (MCMC) method is used [32].

From Eq.(17), we have

$$\mathbb{E}(\Xi(k, C(u, \xi))) = \int_{\Omega} \Xi(k, C(u, \xi)) R(\xi) d\xi \tag{18}$$

where Ω is a measurable set of ξ, while $R(\xi)$ represents the probability density function of ξ. By generating a set of $\{\xi_i\}_i^{N_m}$, the integral term of Eq.(18) can be approximated and we have

$$\mathbb{E}(\Xi(k, C(u, \xi))) = \frac{1}{N_m} \sum_{i=1}^{N_m} \Xi(k, C(u, \xi_i)) \tag{19}$$

where N_m denotes the size of the random sample.

Based on the transformation steps detailed in the previous subsection and the MCMC sampling method, the control chance constraint can be approximated by

$$\frac{1}{N_m} \sum_{i=1}^{N_m} \Xi(k, C(u, \xi_i)) \leq 1 - \epsilon \tag{20}$$

Consequently, the non-deterministic HV entry trajectory optimization model is replaced by a deterministic version which has the form of:

$$\begin{aligned} \text{minimize} \quad & J_1 \quad \text{or} \quad J_2 \\ \text{subject to} \quad & \dot{x} = f(x) + B(x)u \\ & x(t_0) = x_0 \\ & x(t_f) = x_f \\ & \underline{x} \leq x \leq \bar{x} \\ & g(x) \leq \bar{g} \\ & \frac{1}{N_m} \sum_{i=1}^{N_m} \Xi(k, C(u, \xi_i)) \leq 1 - \epsilon \end{aligned} \tag{21}$$

Eq.(21) is a typical optimal control model that can be addressed by well-developed trajectory optimization algorithms using the "discretization + optimization" mode.

4. Convex Chance-Constrained Optimization Approach

It should be noted that according to Eq.(21), the original problem has been transcribed to a deterministic yet nonconvex optimization model. A potential problem of solving a nonconvex optimization problem is that the computation

burden might be high and unpredictable. Fortunately, as suggested by many related works, the convex relaxation-based algorithms are able to address this concern. Therefore, in this section, we focus on designing a convex chance-constrained optimization approach (CCCO) that is capable of solving the considered HV entry problem. Specifically, in Sec 4.1, the convex relaxation of system dynamics and hard constraints is derived. Different from the method presented in Sec 3.1, a convex chance constraint handling method is presented in Sec 4.2. Subsequently, the overall CCCO model is presented in Sec 4.3.

4.1. Convex Relaxation of Dynamics and Hard Constraints

In order to solve problem (21) via convex optimization, one important step is to convexify the nonconvex terms existing in the optimal control model. We firstly consider the terminal cost given by Eq.(10) and Eq.(11) in a more general form $\Phi(x(t_f))$. It should be noted that in some cases, there might exist nonconvexity in the terminal cost $\Phi(x(t_f))$. Hence, convex relaxation is performed on $\Phi(x(t_f))$. More precisely, a first-order Taylor expansion can be executed on $\Phi(x(t_f))$ with respect to a reference terminal point $x_r(t_f)$. That is,

$$\Phi(x(t_f)) \approx \Phi(x_r(t_f)) + F_\Phi(x_r(t_f))(x(t_f) - x_r(t_f)) \tag{22}$$

where

$$F_\Phi(x(t_f)) = \frac{\partial \Phi(x(t_f))}{\partial x(t_f)}$$

Apart from the terminal cost function, another term that needs to be convexified in Eq.(10) is the nonlinear function $f(x)$. Similar with the terminal cost function, to achieve this convex relaxation, the first-order Taylor expansion is used for $f(x)$ with respect to a given reference trajectory $x_r(t)$. This can be written as:

$$f(x) \approx f(x_r) + A(x_r)(x - x_r) \tag{23}$$

where the matrix $A(x) \in \mathbb{R}^{7\times 7}$ can be obtained by partially differentiating $f(x)$ with respect to x. That is, we have

$$A(x) = \frac{\partial f(x)}{\partial x} \tag{24}$$

resulting in

$$A(x) = \begin{bmatrix} 0 & 0 & 0 & a_{14} & a_{15} & 0 & 0 \\ a_{21} & 0 & a_{23} & a_{24} & a_{25} & a_{26} & 0 \\ a_{31} & 0 & 0 & a_{34} & a_{35} & a_{36} & 0 \\ a_{41} & 0 & 0 & a_{44} & a_{45} & 0 & 0 \\ a_{51} & 0 & 0 & a_{54} & a_{55} & 0 & a_{57} \\ a_{61} & 0 & a_{63} & a_{64} & a_{65} & a_{66} & a_{67} \\ 0 & 0 & 0 & 0 & 0 & 0 & a_{77} \end{bmatrix} \tag{25}$$

In Eq.(25), the nonzero terms of a_{ij}, $i, j = 1, ..., 7$ are defined in the Appendix of this paper (see e.g., Appendix A). Consequently, the original nonlinear dynamics has been transformed to

$$\dot{x} \approx f(x_r) + A(x_r)(x - x_r) + Bu \tag{26}$$

By viewing Eq.(5), it is obvious that the path constraint functions are also nonlinear. As a result, efforts have been devoted on transcribing these equations into a convex version. By analogically applying Taylor expansion theory, the convexified path constraint equations can be written as:

$$g(x) \approx g(x_r) + F_g(x_r)(x - x_r) \tag{27}$$

where the matrix $F_g(x) \in \mathbb{R}^{3\times 7}$ can be obtained by partially differentiating $g(x)$ with respect to x, which has the form of

$$F_g(x) = \begin{bmatrix} b_{11} & 0 & 0 & b_{14} & 0 & 0 & 0 \\ b_{21} & 0 & 0 & b_{24} & 0 & 0 & 0 \\ b_{31} & 0 & 0 & b_{34} & 0 & 0 & 0 \end{bmatrix} \tag{28}$$

In Eq.(28), the nonzero terms b_{ij}, $i = 1, ..., 3$ and $j = 1, ..., 7$ are included in the Appendix of this paper.

4.2. Convex Approximation of Control Chance Constraint

From the definition of the chance constraint approximation function given by Eq.(16), it is obvious that $\Xi(k, C(u, \xi))$ is nonconvex. To preserve the convexity of the problem, it is desired to seek an alternative convex approximation function $\Xi_c(C(u, \xi))$ to replace the function $H(C(u, \xi))$ in Eq.(15). In this paper, we suggest a convex function in the form of

$$\Xi_c(C(u, \xi)) = \max(C(u, \xi) + 1, 0) \tag{29}$$

where the term $\max(C(u,\xi)+1,0)$ returns the greater value between $C(u,\xi)+1$ and 0.

It can be verified that the convex function given by Eq.(29) is strictly greater than the unit step function H, thereby forming in an upper estimation of the original chance constraint. Similar with the process detailed in Sec 3.2, the expectation value of $\Xi_c(C(u,\xi))$ and the original control chance constraint can be approximated by Eq.(30) and Eq.(31), respectively.

$$\mathbb{E}(\Xi_c(C(u,\xi))) = \frac{1}{N_m}\sum_{i=1}^{N_m}\Xi_c(C(u,\xi_i)) \tag{30}$$

$$\frac{1}{N_m}\sum_{i=1}^{N_m}\Xi_c(C(u,\xi_i)) \leq 1-\epsilon \tag{31}$$

4.3. Overall CCCO Model

According to the convex relaxation processes acted on the nonlinear dynamics, path constraints, objective functions, and control chance constraints, a CCCO model can be constructed which is in the form of:

$$\begin{aligned}
\text{minimize} \quad & \Phi(x_r(t_f)) + F_\Phi(x_r(t_f))(x(t_f)-x_r(t_f)) \\
\text{subject to} \quad & \dot{x} = f(x_r) + A(x_r)(x-x_r) + Bu \\
& x(t_0) = x_0 \\
& x(t_f) = x_f \\
& \underline{x} \leq x \leq \bar{x} \\
& g(x_r) + F_g(x_r)(x-x_r) \leq \bar{g} \\
& \frac{1}{N_m}\sum_{i=1}^{N_m}\Xi_c(C(u,\xi_i)) \leq 1-\epsilon \\
& \|x-x_r\| \leq \varrho
\end{aligned} \tag{32}$$

Remarkably, the convexity of inequality (29), together with the convexity of the locally linearized objectives, system dynamics and constraints, guarantees the convexity of the optimization model (32). It is also worth noting that a trust-region constraint $\|x-x_r\| \leq \varrho$ is imposed on the optimization in order to guarantee the effectiveness of the linearization process performed for the objective, system dynamics and constraints.

Based on the CCCO model, we are able to construct a successive convex trajectory optimization process:

Step 1. Assign the initial condition for system state variables $x(t_0) = x_0$.

Step 2. Calculate the initial state reference trajectory $x_r^{(k)}$ by using x_0 and the initial control reference u_r^k.

Step 3. Generate a set of random samples $\{\xi_i\}_i^{N_m}$ and construct the convex approximation function (29).

Step 4. Search the optimal solution (x^k, u^k) of the optimization model (32).

Step 5. Check the condition for termination via $\|x^k - x_r^{(k)}\| \leq \varepsilon$. If the condition can be satisfied, then jump to Step 6. Otherwise, assign $x_r^{(k)} = x^k$, $u_r^{(k)} = u^k$, set $k = k + 1$ and jump to Step 4.

Step 6. Output the solution (x^k, u^k).

5. Performance Evaluation

In this section, the performance and validity of the proposed NCCO and CCCO algorithms are demonstrated for solving the chance-constrained HV entry optimization problem, respectively.

5.1. Parameters and Mission Cases Specification

The vehicle and environment-related parameters are similar to the configurations examined in [3]. Specifically, the mass and reference area of the spacecraft are assigned as 92079kg and 249.91m^2, whereas the isothermal atmospheric model given by (4) is used to simulate the atmospheric flight. In the simulation, we mainly consider the following two test cases:

- Mission case 1: Cross-range optimal trajectory planning;
- Mission case 2: Time-optimal trajectory planning.

Both of the above two mission cases apply the same initial and terminal conditions which are tabulated in Table 2. Besides, other mission-related parameters such as the maximum allowable variable bounds and path constraint values are also included in Table 2. Aerodynamic parameters such as the lift and drag coefficients (C_L, C_D) are approximated via the following equation [3, 31]:

$$\begin{aligned} C_D &= C_{D_0} + C_{D_1}\alpha + C_{D_2}\alpha^2 \\ C_L &= C_{L_0} + C_{L_1}\alpha \end{aligned} \tag{33}$$

Table 2: Parameter assignment

Parameters	Values	Parameters	Values/Ranges
h_0, m	80	$\bar{P}_d$, N/m^2	18000
θ_0, deg	0	$\bar{N}_L$, g	2.5
ϕ_0, deg	0	h_f, m	25
V_0, m/s	7800	V_f, m/s	750
γ_0, deg	-1	γ_f, deg	-5
ψ_0, deg	0	σ, deg	[-90, 1]
σ_0, deg	-75	σ_c, deg	[-90, 1]
$\bar{Q}$, Btu	200	t, s	[0, 2000]

in which α stands for the angle of attack (AOA) and its value can be obtained via [28]:

$$\alpha = \begin{cases} 40 - w_1(V - 4570)^2/340^2, & \text{if } V < 4570m/s; \\ 40, & \text{if } V \geq 4570m/s. \end{cases} \tag{34}$$

where $w_1 = 0.20705$. As for the control chance constraint, according to Eq.(20), the bank angle chance constraint is transcribed to

$$\mathbb{E}_{\xi_\sigma}(\Psi(k, \sigma_c + \xi_\sigma - \bar{\sigma}_c)) \leq 1 - \epsilon_\sigma \tag{35}$$

In Eq.(35), the maximum allowable constraint violation level $1 - \epsilon_\sigma$ is set to 10%, whereas the uncertain parameter ξ_σ is supposed to have an exponential distribution $R(z; \lambda) = \lambda e^{-\lambda z}$, where $z \geq 0$ and $\lambda = 0.5$. For the nonconvex chance-constraint approximation strategy, m_1 and m_2 are assigned to 1.0 and 0.5, respectively. Furthermore, the sizes of the temporal set and MCMC sample set are specified as $N_k = 100$ and $N_m = 2 \times 10^4$, respectively.

5.2. NCCO Results and Discussions

The performance of using the NCCO formulation constructed in Sec 3 is firstly examined. It should be clarified that both the NCCO and CCCO algorithms solve the same entry mission cases. In NCCO the original system dynamics, path constraints and the approximated chance constraint (20) are considered, while in CCCO the convexified dynamics (26), path constraints (27) and chance constraint (31) are included in the optimization process. Based

on the parameters and setting detailed in the previous subsection, the optimal results for both test cases are produced and visualized in Fig. 1 to Fig. 6. More precisely, Figs. 1-3 describe, respectively, the obtained system state evolutions, path constraints profiles, and the control and chance constraint violation histories for mission case 1. Similarly, for mission case 2, the corresponding trajectories are presented in Figs. 4-6. By viewing the state and path constraint trajectories (e.g., Fig.1, Fig.2, Fig.4, and Fig.5), all the targeted final conditions can be achieved and the path constraints are able to stay in the acceptable corridors, thus confirming the validity of the obtained results. In addition, from the evolution profiles shown in Fig.3 and Fig.6, the violation rates of σ_c are always smaller than the level parameter $1 - \epsilon_\sigma$, thereby reflecting the effectiveness of the chance constraint handling method.

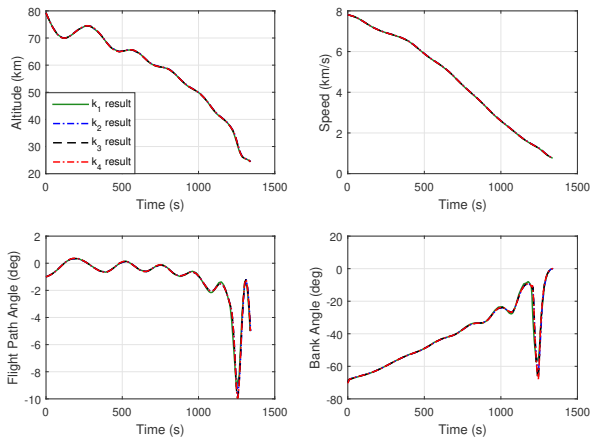

Figure 1: System state evolutions: Case 1 (NCCO Results)

As discussed in Sec 3, a key parameter that could have effects on the algorithm performance is the constant k. Therefore, we perform a study to further analyze the sensitivity of k with respect to the optimal solutions. By setting $k = [k_1, k_2, k_3, k_4]$=[50, 200, 350, 500], simulations were performed for both case 1 and case 2. The calculated trajectory profiles are also reported in Figs.1-6, while detailed results including the maximum path constraint/violation rate values achieved, and the algorithm execution time t_p are summarised and tabulated in Table 3.

From the results reported in Figs.1-3 and Table 3, it can be seen that the

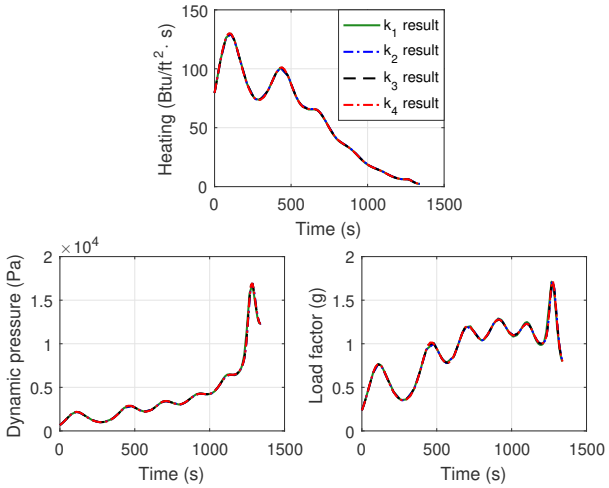

Figure 2: Path constraints profiles: Case 1 (NCCO Results)

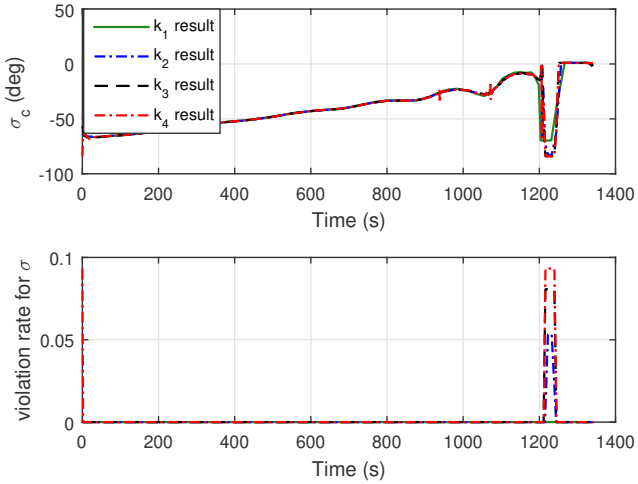

Figure 3: Control/Chance constraint histories: Case 1 (NCCO Results)

variance of k is not sensitive with respect to the cross-range optimal results. Interestingly, more obvious differences can be detected from the results of mission case 2 (e.g., see Figs.4-6 and Table 3, the time-optimal case 2). A higher value k tends to result in a more aggressive control chance constraint violation history, thereby reducing more conservatism during the optimization process.

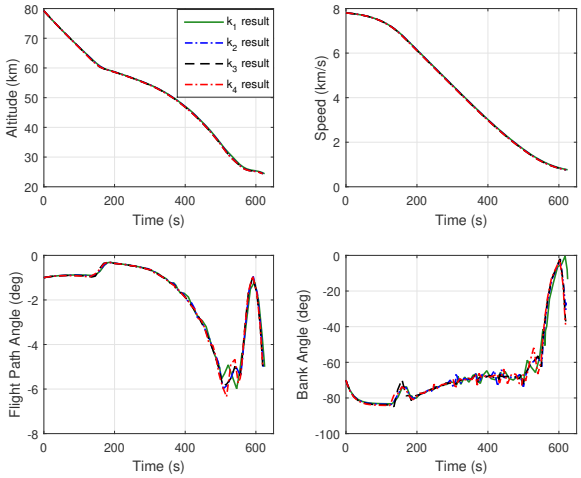

Figure 4: System state evolutions: Case 2 (NCCO Results)

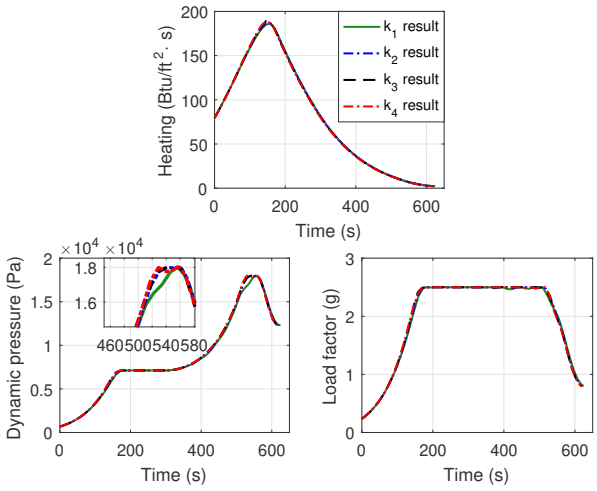

Figure 5: Path constraints profiles: Case 2 (NCCO Results)

This aggressive behaviour can also be reflected by the dynamic pressure evolution profiles. That is, by setting $k = k_4$, the P_d value reaches its peak value $\bar{P}_d$ at about 510s, while this time is postponed to around 560s for k_1-based results. As a consequence, we can observe a trend that the objective value becomes more optimal as the value of k goes higher. On the other hand, it is not always

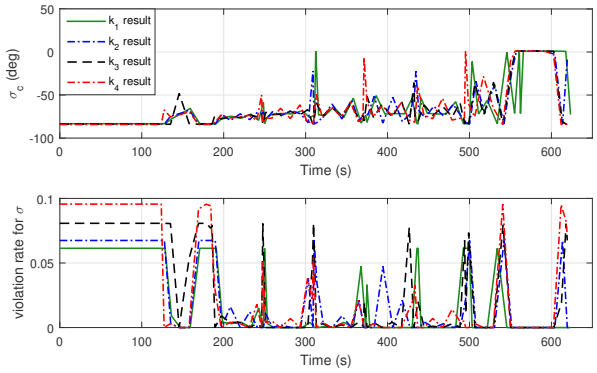

Figure 6: Control/Chance constraint histories: Case 2 (NCCO Results)

Table 3: Detailed results for NCCO

NCCO Results	Case 1			
	k_1	k_2	k_3	k_4
$\max Q$, Btu	129.79	129.33	129.85	130.13
$\max P_d$, N/m^2	16813	16958	16943	16942
$\max N_L$, g	1.71	1.72	1.72	1.72
$\max Vio$, %	0.81	5.34	7.47	9.32
J_1^*, deg	16.34	16.35	16.35	16.36
t_p, s	24.37	28.52	27.17	35.56
NCCO Results	Case 2			
	k_1	k_2	k_3	k_4
$\max Q$, Btu	185.89	186.61	189.07	189.41
$\max P_d$, N/m^2	18000	18000	18000	18000
$\max N_L$, g	2.50	2.50	2.50	2.50
$\max Vio$, %	6.14	6.75	8.07	9.56
J_2^*, s	624.70	624.64	619.37	616.92
t_p, s	55.58	59.90	61.12	77.55

good to select a higher value of k for the NCCO algorithm. From the processing time results shown in Table 3, it is clear that using a higher value of k tends to increase the algorithm execution time. This might be caused by multiple factors such as the numerical difficulty or tightness of the feasible solution space.

In summary, based on these results shown earlier, we conclude that a main advantage of using the NCCO approach presented in Sec 3 is that the probabilistic constraint imposed on the control variable can be aggressively ensured. Hence, it is possible to reduce the conservatism and offer more optimality to the obtained solution.

5.3. CCCO Results and Discussions

In this subsection, the performance of using CCCO method developed in Sec 4 to solve the considered problem is analyzed. Moreover, studies were carried out to compare the results obtained via the NCCO and CCCO methods.

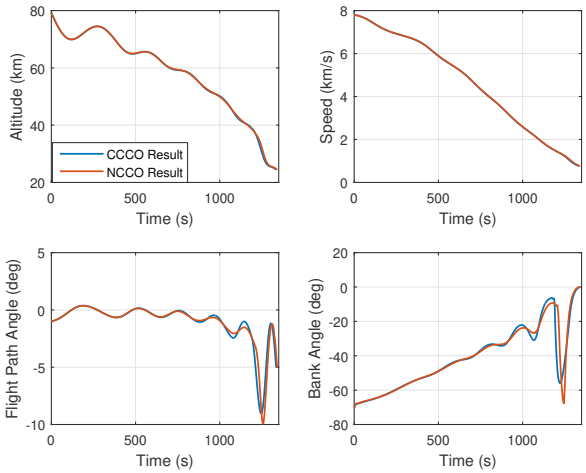

Figure 7: System state evolutions: Case 1 (CCCO Results)

Table 4: Detailed results for CCCO

Results	Case 1	Case 2
$\max Q$, Btu	130.45	183.74
$\max P_d$, N/m^2	17125	18000
$\max N_L$, g	1.77	2.5
$\max Vio$, %	5.03	5.09
J_2^*, s	16.29	631.98
t_p, s	6.47	7.32

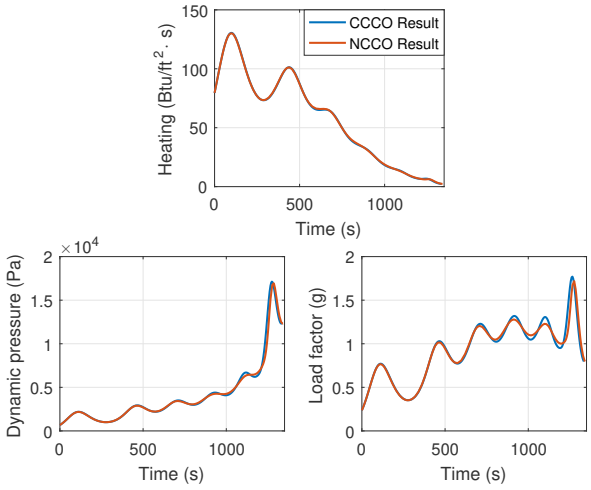

Figure 8: Path constraints profiles: Case 1 (CCCO Results)

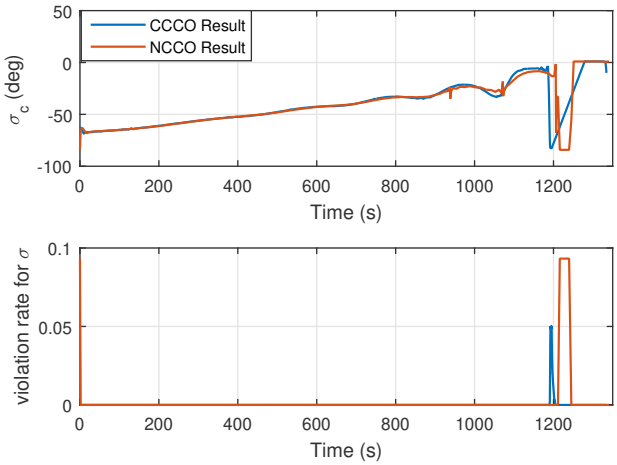

Figure 9: Control/Chance constraint histories: Case 1 (CCCO Results)

Comparative time histories of the system state variables and path constraints for the two mission case are displayed in Figs.7-8 and Figs.10-11, from where it can be seen that the optimal solutions obtained via the NCCO and CCCO are similar. In addition, by viewing Fig.8 and Fig.11, the path constraint profiles obtained via the two proposed methods can always be restricted

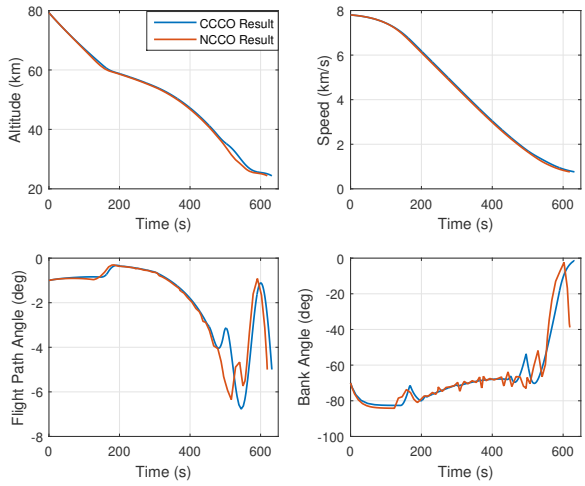

Figure 10: System state evolutions: Case 2 (CCCO Results)

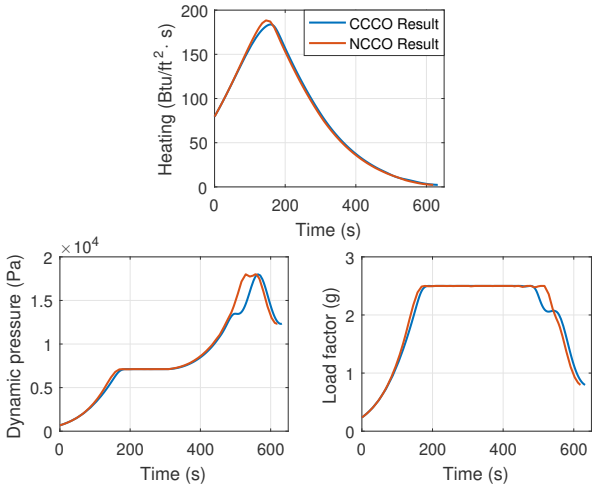

Figure 11: Path constraints profiles: Case 2 (CCCO Results)

in their tolerant corridors, thereby ensuring the flight safety.

The actual and demanded bank angle $[\sigma, \sigma_c]$ are shown in Fig.9 and Fig.12, respectively. Significant differences can be detected from the control evolution files obtained via NCCO and CCCO. This is partly cased by the chance constraint approximation strategy used in the two optimization model. Certainly,

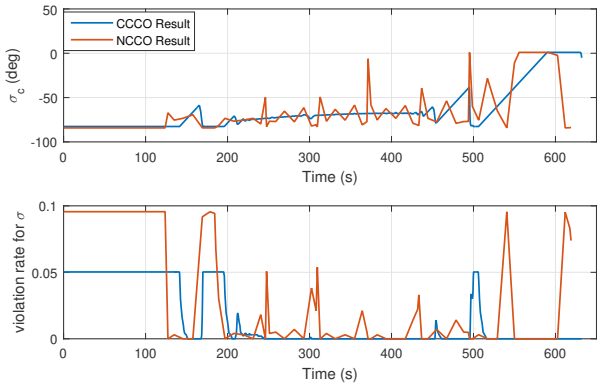

Figure 12: Control/Chance constraint histories: Case 2 (CCCO Results)

the chance constraint handling strategy used in the NCCO formulation can result in more aggressive approximation performance and more optimal objective value. However, it will significantly increase the computational time required for convergence. Specifically, detailed execution performance of applying CCCO for the two mission cases are reported in Table 4. By comparing the results reported in Table 3 and Table 4, two main conclusions can be made. Firstly, using the convex approximation-based chance constraint handling method can successfully ensure the violation rate of Eq.(35) is less than the level parameter $\varepsilon = 0.1$ (10%). Secondly, although the CCCO algorithm tends to result in higher conservatism in comparison to the NCCO, the computational performance of applying the CCCO is much better than that of the NCCO. This is attributed by the guaranteed polynomial-time complexity of CCCO, while the processing complexity of using the NCCO is hard to predict.

In addition, a noteworthy point from the comparative results can be observed from these control evolution profiles. That is, the CCCO algorithm tends to result in a σ_c control sequence with less oscillations or instant variations, thereby further smoothing the actual bank angle profile. This trend becomes more obvious when using the proposed methods to address mission case 2, as the optimal control structure for this mission case should ideally keep a bang-singular-bang mode.

It should be noted that while using the convexified formulation given by Eq.(32) can achieve enhanced computational performance, it is not always ad-

vantageous to transcribe a nonconvex trajectory optimization model into a convex version. For some trajectory optimization problems, the convex relaxation process can result in significant mismatches between the convexified system and the original one, thereby damaging the effectiveness and reliability of the calculated results. Alternatively, the nonconvex chance-constrained formulation (21) and widely-applied NLP solvers can be a good candidate to solve these flight path design problems under parameter uncertainties.

6. Conclusion

In this work, an attempt to research the problem of hypersonic vehicle atmospheric entry under a complex environment was presented. Due to the simultaneous existence of hard and probabilistic path constraints, the corresponding trajectory optimization model becomes challenging to solve. To effectively explore the optimal control profile, we established and implemented two chance-constrained trajectory optimization methods. Both of the proposed methods have the flexibility to transcribe the original chance-constrained optimal control problem into a deterministic version, which is solvable for general NLP solvers or convex optimization methods. Key features of the proposed designs were illustrated by performing a number of numerical simulations. Based on the obtained results, we have observed that the optimal solution has a bang-bang structure and the proposed methods can produce near-optimal solutions while satisfying different types of constraints. In addition, using the convex-relaxed design can generally improve the computational performance of the algorithm, thereby narrowing the gap between offline simulation and online implementation. Consequently, we suggest applying the proposed designs to plan the flight trajectory for the hypersonic vehicle during the atmospheric entry flight. In future research, more complex mission-related chance constraints will be included in the designed NCCO and CCCO model. For instance, the uncertain no-fly zone constraints which commonly exist in practical scenarios are desired to be taken into account. Accordingly, a proper treatment is required to reformulate this type of constraint to a convex form, thereby preserving the convexity of the CCCO model.

Appendix

Nonzero components of $A(x)$ are defined in the following equations:

$$\begin{aligned}
a_{14} &= \sin\gamma & a_{15} &= V\cos\gamma \\
a_{21} &= -\tfrac{V\cos\gamma\sin\psi}{r^2\cos\phi} & a_{23} &= \tfrac{V\cos\gamma\sin\psi\tan\phi}{r\cos\phi} \\
a_{24} &= \tfrac{\cos\gamma\sin\psi}{r\cos\phi} & a_{25} &= -\tfrac{V\cos\gamma\sin\psi}{r\cos\phi} \\
a_{26} &= \tfrac{V\cos\gamma\cos\psi}{r\cos\phi} & a_{31} &= -\tfrac{V\cos\gamma\cos\psi}{r^2} \\
a_{34} &= \tfrac{\cos\gamma\cos\psi}{r} & a_{35} &= -\tfrac{V\cos\gamma\cos\psi}{r} \\
a_{36} &= -\tfrac{V\cos\gamma\sin\psi}{r} & a_{41} &= \tfrac{kC_DV^2}{H} + \tfrac{2g\sin\gamma}{r} \\
a_{44} &= -2kC_DV & a_{45} &= -g\cos\gamma
\end{aligned} \tag{A.1}$$

$$\begin{aligned}
a_{51} &= -V(\tfrac{kC_L\cos\sigma}{h_s} + \tfrac{\cos\gamma}{r^2}) + \tfrac{2g\cos\gamma}{Vr} \\
a_{54} &= kC_L\cos\sigma + \tfrac{gr+V^2}{V^2r}\cos\gamma \\
a_{55} &= \sin\gamma\tfrac{gr-V^2}{Vr} \\
a_{57} &= -\tfrac{L\cos\sigma}{V} \\
a_{61} &= -V(\tfrac{kC_L\sin\sigma}{H\cos\gamma} + \tfrac{\cos\gamma\sin\psi\tan\theta}{r^2}) \\
a_{63} &= \tfrac{V\cos\gamma\sin\psi}{r}(1+\tan^2\theta) \\
a_{64} &= \tfrac{kC_L\sin\sigma}{\cos\gamma} + \tfrac{\cos\gamma\sin\psi\tan\theta}{r} \\
a_{65} &= \tfrac{V\tan\gamma kC_L\sin\sigma}{\cos\gamma} - \tfrac{V\sin\gamma\sin\psi\tan\theta}{r} \\
a_{66} &= \tfrac{V\cos\gamma\tan\theta\cos\psi}{r} \\
a_{67} &= \tfrac{L\cos\sigma}{V\cos\gamma} \\
a_{77} &= K \\
k &= \rho S/2m
\end{aligned} \tag{A.2}$$

Besides, the nonzero components of $F_g(x)$ are defined in Eq.(A.3)

$$\begin{aligned}
b_{11} &= \tfrac{1}{2}k_QV^{3.15}\sqrt{\rho}/h_s \\
b_{14} &= 3.15k_QV^{2.15}\sqrt{\rho} \\
b_{21} &= \tfrac{1}{2}\rho V^2/h_s \\
b_{24} &= \rho V \\
b_{31} &= \tfrac{1}{2}\rho V^2S\sqrt{C_L^2+C_D^2}/mgh_s \\
b_{34} &= S\sqrt{C_L^2+C_D^2}/mg
\end{aligned} \tag{A.3}$$

References

[1] N. N. Smirnov, Space flight safety: experiments and supercomputing, Acta Astronautica 163 (2019) 1–5. doi:https://doi.org/10.1016/j.actaastro.2019.08.021.

[2] L. Pan, S. Peng, Y. Xie, Y. Liu, J. Wang, 3d guidance for hypersonic reentry gliders based on analytical prediction, Acta Astronautica 167 (2020) 42–51. doi:https://doi.org/10.1016/j.actaastro.2019.07.039.

[3] R. Chai, A. Savvaris, A. Tsourdos, Violation learning differential evolution-based hp-adaptive pseudospectral method for trajectory optimization of space maneuver vehicle, IEEE Transactions on Aerospace and Electronic Systems 53 (4) (2017) 2031–2044. doi:10.1109/TAES.2017.2680698.

[4] C. Chawla, P. Sarmah, R. Padhi, Suboptimal reentry guidance of a reusable launch vehicle using pitch plane maneuver, Aerospace Science and Technology 14 (6) (2010) 377–386. doi:http://dx.doi.org/10.1016/j.ast.2010.04.001.

[5] R. Chai, A. Savvaris, A. Tsourdos, S. Chai, Y. Xia, Improved gradient-based algorithm for solving aeroassisted vehicle trajectory optimization problems, Journal of Guidance, Control, and Dynamics 40 (8) (2017) 2093–2101. doi:10.2514/1.G002183.

[6] H. Zhou, X. Wang, N. Cui, Glide trajectory optimization for hypersonic vehicles via dynamic pressure control, Acta Astronautica 164 (2019) 376–386. doi:https://doi.org/10.1016/j.actaastro.2019.08.012.

[7] W. W. Hager, H. Hou, A. V. Rao, Convergence rate for a gauss collocation method applied to unconstrained optimal control, Journal of Optimization Theory and Applications (2016) 1–24doi:10.1007/s10957-016-0929-7.

[8] C. L. Darby, W. W. Hager, A. V. Rao, Direct trajectory optimization using a variable low-order adaptive pseudospectral method, Journal of Spacecraft and Rockets 48 (3) (2011) 433–445. doi:10.2514/1.52136.

[9] F. Fahroo, I. M. Ross, Pseudospectral methods for infinite-horizon nonlinear optimal control problems, Journal of Guidance, Control, and Dynamics 31 (4) (2008) 927–936. doi:10.2514/1.33117.

[10] D. Garg, M. Patterson, W. W. Hager, A. V. Rao, D. A. Benson, G. T. Huntington, A unified framework for the numerical solution of optimal control problems using pseudospectral methods, Automatica 46 (11) (2010) 1843–1851. doi:http://dx.doi.org/10.1016/j.automatica.2010.06.048.

[11] Y. Mao, D. Zhang, L. Wang, Reentry trajectory optimization for hypersonic vehicle based on improved gauss pseudospectral method, Soft Computing 21 (16) (2017) 4583–4592. doi:10.1007/s00500-016-2201-3.

[12] B. A. Conway, A survey of methods available for the numerical optimization of continuous dynamic systems, Journal of Optimization Theory and Applications 152 (2) (2012) 271–306. doi:10.1007/s10957-011-9918-z.

[13] H. Duan, S. Li, Artificial bee colony based direct collocation for reentry trajectory optimization of hypersonic vehicle, IEEE Transactions on Aerospace and Electronic Systems 51 (1) (2015) 615–626. doi:10.1109/TAES.2014.120654.

[14] J. A. Englander, B. A. Conway, Automated solution of the low-thrust interplanetary trajectory problem, Journal of Guidance, Control, and Dynamics 40 (1) (2017) 15–27. doi:10.2514/1.G002124.

[15] J. J. Kim, J. J. Lee, Trajectory optimization with particle swarm optimization for manipulator motion planning, IEEE Transactions on Industrial Informatics 11 (3) (2015) 620–631. doi:10.1109/TII.2015.2416435.

[16] M. Pontani, B. A. Conway, Minimum-fuel finite-thrust relative orbit maneuvers via indirect heuristic method, Journal of Guidance, Control, and Dynamics 38 (5) (2014) 913–924. doi:10.2514/1.G000157.

[17] N. Yokoyama, S. Suzuki, Modified genetic algorithm for constrained trajectory optimization, Journal of Guidance, Control, and Dynamics 28 (1) (2005) 139–144. doi:10.2514/1.3042.

[18] W. Zou, P. Shi, Z. Xiang, Y. Shi, Consensus tracking control of switched stochastic nonlinear multiagent systems via event-triggered strategy, IEEE Transactions on Neural Networks and Learning Systems 31 (3) (2020) 1036–1045. doi:10.1109/TNNLS.2019.2917137.

[19] Z. Wu, H. R. Karimi, P. Shi, Practical trajectory tracking of random lagrange systems, Automatica 105 (2019) 314–322. doi:https://doi.org/10.1016/j.automatica.2019.04.006.

[20] J. Xu, P. Shi, C. Lim, C. Cai, Y. Zou, Reliable tracking control for underactuated quadrotors with wind disturbances, IEEE Transactions on Sys-

tems, Man, and Cybernetics: Systems 49 (10) (2019) 2059–2070. doi:10.1109/TSMC.2017.2782662.

[21] T. Chan, P. Mar, Stability and continuity in robust optimization, SIAM Journal on Optimization 27 (2) (2017) 817–841. doi:10.1137/16M1067512.

[22] D. GonzAlez-Arribas, M. Soler, M. Sanjurjo-Rivo, Robust aircraft trajectory planning under wind uncertainty using optimal control, Journal of Guidance, Control, and Dynamics (2017) 1–16doi:10.2514/1.G002928.

[23] R. Chai, A. Savvaris, A. Tsourdos, S. Chai, Y. Xia, S. Wang, Solving trajectory optimization problems in the presence of probabilistic constraints, IEEE Transactions on Cybernetics (2019) 1–14doi:10.1109/TCYB.2019.2895305.

[24] A. Geletu, A. Hoffmann, M. Kloppel, P. Li, An inner-outer approximation approach to chance constrained optimization, SIAM Journal on Optimization 27 (3) (2017) 1834–1857. doi:10.1137/15M1049750.

[25] J. B. Caillau, M. Cerf, A. Sassi, E. Trelat, H. Zidani, Solving chance constrained optimal control problems in aerospace via kernel density estimation, Optimal Control Applications and Methods 39 (5) (2018) 1833–1858. doi:10.1002/oca.2445.

[26] Z. Zhao, M. Kumar, Split-bernstein approach to chance-constrained optimal control, Journal of Guidance, Control, and Dynamics 40 (11) (2017) 2782–2795. doi:10.2514/1.G002551.

[27] X. Liu, Z. Shen, P. Lu, Exact convex relaxation for optimal flight of aerodynamically controlled missiles, IEEE Transactions on Aerospace and Electronic Systems 52 (4) (2016) 1881–1892. doi:10.1109/TAES.2016.150741.

[28] Z. Wang, M. J. Grant, Constrained trajectory optimization for planetary entry via sequential convex programming, Journal of Guidance, Control, and Dynamics 40 (10) (2017) 2603–2615. doi:10.2514/1.G002150.

[29] D.-J. Zhao, Z.-Y. Song, Reentry trajectory optimization with waypoint and no-fly zone constraints using multiphase convex programming, Acta Astronautica 137 (2017) 60–69. doi:https://doi.org/10.1016/j.actaastro.2017.04.013.

[30] R. Chai, A. Savvaris, A. Tsourdos, Fuzzy physical programming for space manoeuvre vehicles trajectory optimization based on hp-adaptive pseudospectral method, Acta Astronautica 123 (2016) 62–70. doi:http://dx.doi.org/10.1016/j.actaastro.2016.02.020.

[31] T. R. Jorris, R. G. Cobb, Three-dimensional trajectory optimization satisfying waypoint and no-fly zone constraints, Journal of Guidance, Control, and Dynamics 32 (2) (2009) 551–572. doi:10.2514/1.37030.

[32] P. Constantine, C. Kent, T. Bui-Thanh, Accelerating markov chain monte carlo with active subspaces, SIAM Journal on Scientific Computing 38 (5) (2016) A2779–A2805. doi:10.1137/15M1042127.

Trajectory planning for hypersonic reentry vehicle satisfying deterministic and probabilistic constraints

Chai, Runqi

2020-07-02

Chai R, Tsourdos A, Savvaris A, et al., (2020) Trajectory planning for hypersonic reentry vehicle satisfying deterministic and probabilistic constraints. Acta Astronautica, Volume 177, December 2020, pp. 30-38

https://doi.org/10.1016/j.actaastro.2020.06.051